Materials Science in Semiconductor Processing 30 (2015) 292–297

Contents lists available at ScienceDirect

Materials Science in Semiconductor Processing

journal homepage: www.elsevier.com/locate/mssp

Optimising conditions for the growth of nanocrystalline ZnS thin films from acidic chemical baths

Muhammad Saeed Akhtar [a,c], Mohammad Azad Malik [a,*], Saira Riaz [c], Shahzad Naseem [c], Paul O'Brien [a,b]

[a] School of Materials, The University of Manchester, Oxford Road, Manchester M13 9 PL, UK
[b] School of Chemistry, The University of Manchester, Oxford Road, Manchester M13 9 PL, UK
[c] Centre of Excellence in Solid State Physics, University of the Punjab, Lahore 54590, Pakistan Schools of Chemistry and Materials, The University of Manchester, Oxford Road, Manchester M13 9 PL, UK

ARTICLE INFO

Available online 7 November 2014

Keywords:
Chemical bath deposition
Zinc sulfide
Thin films
Nanoparticles
p-XRD

ABSTRACT

The growth of nanocrystalline zinc sulfide thin films onto glass substrates by chemical bath deposition has been optimized at acidic pH. Powder X-ray diffraction (p-XRD) confirms the deposition of sphalerite, the cubic phase of ZnS. The crystallite size calculated by Scherrer equation was found to be 4.0 nm. Scanning Electron Microscopy (SEM) show clusters of spherical nanoparticles uniformly distributed over the surface of the glass substrates. Energy Dispersive X-ray (EDX) analysis of the deposited thin films show the zinc to sulfur ratio close to 1:1. The observed band gap (3.78 eV) of the deposited thin films is higher than that reported for cubic phase of bulk ZnS (3.54 eV) as expected due to nano-size crystallites. Binding energies calculated by X-ray Photoelectron Spectroscopy (XPS) confirm the material as ZnS and the photoluminescence measurements show the blue shift in emission maximum.

1. Introduction

Zinc sulfide is a relatively benign wide band gap semiconductor material. It has applications in photonic crystal sensors [1], heterojunction diodes [2], thin film photovoltaic cells [3–7], optical filters [8], light emitting diodes [9] and anti-reflection coatings [10]. Several methods have been employed to synthesize thin films including spray pyrolysis [11,12], solvothermal synthesis [13,14], sol–gel [2], successive ionic layer adsorption and reaction (SILAR) [15], pulsed laser deposition [16], close-space sublimation [17], metal-organic chemical vapor deposition (MOCVD), photo-assisted MOCVD [18], RF-mganetron sputtering [19,20], electrodeposition [21,22], thermal evaporation [23], aerosol assisted chemical vapor deposition (AACVD) [24,25], chemical bath deposition (CBD) [26–34] and film casting method [35,36]. Among these, CBD is potentially a simple, low temperature and cost effective method to high quality thin films.

Although there are many reports on the deposition of ZnS thin films by CBD, most show the deposition of either amorphous ZnS or a mixture of ZnS and ZnO [37,38]. Long et al. [39] reported an improved method for deposition of ZnS thin films by CBD on pre-heated substrates. O'Brien et al. [40] discussed the strategies needed to obtain high quality ZnS thin films by CBD. The effect of different complexing agents has also been explored [32,41]. Recent reports discuss the effect of different deposition variables on structural and optical properties of ZnS thin films obtained from CBD [42–45]. Despite considerable efforts

* Corresponding author. Tel.: +44 161 2751411.
E-mail address: azad.malik@manchester.ac.uk (M.A. Malik).

http://dx.doi.org/10.1016/j.mssp.2014.10.019
1369-8001/

to understand the precise control of the crystal phase, degree of crystallinity, stoichiometric composition and morphology, there remains a challenge.

We report a reproducible method for the deposition of nanocrystalline monophasic ZnS thin films with controlled morphology and stoichiometry. Growth parameters for deposition of thin films have been optimized and the reproducibility of the results has been verified through repeated experiments.

2. Experimental section

2.1. Chemicals

All reagents, zinc chloride (≥ 98%), thioacetamide (≥ 99%) and urea (≥ 99%) were purchased from Sigma-Aldrich and used without further purification. De-ionized water was used in all experiments. Acetone and 2-propanol were used for cleaning the substrate.

2.2. Instruments

A Mettler Toledo meter calibrated against standard pH 2.00, 4.01, and 7.00 buffers was used to record pH. X-ray powder diffraction measurements were performed using a Bruker D8 advance diffractometer with Cu-Kα radiation. Data were recorded for three hours scan across a 2θ range of 20–80°, using a step size of 0.02°. SEM and EDAX analyses were carried out using a Philips XL 30 microscope. To avoid charging, samples were carbon coated with a Precision Etching Coating System (682). TEM, HRTEM and SAED images were collected from a Techni 20 F30 transmission electron microscope using accelerating voltage of 200 kV. An atomic force microscope (AFM) PeakForce QNM was used to measure surface roughness of the ZnS thin films. Absorbance and transmittance spectra were acquired using a Agilent HP 8453 UV–vis spectrophotometer.

2.3. Synthesis of ZnS thin films

The ZnS thin films were grown on glass substrates from acidic bath containing zinc chloride (0.15 M), urea (5 M) and thioacetamide (1 M). The solutions of zinc chloride (30 mL), thioacetamide (30 mL), and urea (20 mL) were mixed in a beaker to get total volume of 80 mL bath solution. The pH of bath solution was adjusted to 4.0 by the drop wise addition of 1.0 M HCl. The stirred bath solution was maintained at a temperature of 80 °C. Glass substrates (cleaned ultrasonically by acetone, 2-propanol and de-ionized water for ten minutes each) were immersed vertically in the chemical bath after few minutes of visible turbidity. Substrates were removed from the bath after 3 h, washed and sonicated in de-ionized water to remove any non-adherent particulates. As-deposited films were adherent transparent white. The films were allowed to dry under ambient conditions before characterization.

3. Results and discussion

Reproducibility of the results in CBD experiments have been an issue due to variations in phase, composition and effect of the substrate used. The uniformity and smoothness of the films is also desired due to its important role in properties of the devices fabricated from ZnS thin films. Previously, we have reported the growth of hexagonal ZnS thin films on low iron content glass substrates by CBD using slightly lower pH (3.8) and much lower concentrations of starting materials *i.e.* zinc chloride (0.02 mol dm^{-3}), urea (0.05 mol dm^{-3}) and thioacetamide (0.2 mol dm^{-3}) [34]. In the present work ZnS thin films were grown on glass substrates using solutions of much higher concentration of zinc chloride (0.15 M), urea (5 M) and thioacetamide (1 M) at pH 4.0. Multiple depositions were required to get thick enough films for p-XRD characterization. The ZnS films deposited in this work are cubic phase in contrast to those reported earlier [34]. Films were reproducibly deposited on soda glass, low iron content glass, ITO coated glass and silicon substrates.

3.1. Structural studies

The deposited ZnS films from CBD showed very weak and broad p-XRD peaks, so multi-deposition experiments were carried out on the same glass substrate. The p-XRD pattern of the films deposited after two depositions showed strong diffraction peaks corresponding to cubic ZnS. Subsequent depositions gradually enhanced the intensity of p-XRD pattern (Fig. 1). The observed diffraction peaks in all depositions correspond to (111), (220) and (311) lattice planes of cubic phase and are well matched with reported data (ICSD # 01-080-0020). No diffraction peaks other than ZnS were detected. The broad peaks show the nanocrystalline nature of the deposited films. The broad hump observed between 2θ values of 20–25° is due to glass substrate.

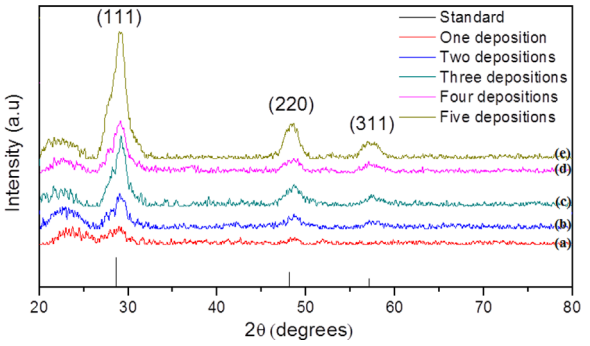

Fig. 1. p-XRD pattern of CBD-deposited ZnS films, onto glass substrates using ([Zn^{2+}]=0.15 M, [Urea]=5 M, [Thioacetamide]=1 M, pH 4, deposition time=3 h). (a)–(e) First deposition to fifth deposition respectively.

Table 1
Comparison of observed *d*-values and lattice constant with the standard.

a (Å) Observed	*a* (Å) Standard	*d* (Å) Observed	*d* (Å) Standard	(*hkl*)
5.3287	5.3450	3.07654	3.08594	111
		1.87959	1.88974	220
		1.60222	1.61158	311

The average crystallite size was (4.0 nm) estimated at FWHM of most intense peak (111) by the Scherrer formula. The lattice parameters calculated are $a=5.32$ Å, which are close to the literature for bulk. The comparison of observed d-values and lattice constant with the standard ones is given in Table 1.

3.2. Morphology and stoichiometry

The SEM micrographs at different magnifications for the ZnS thin film after five depositions are shown in Fig. 2. Low magnification images indicate the uniform distribution of spherical nanoparticles throughout the substrate surface. The apparent crystallite size ranges from 65 nm to 80 nm and the size grow with each deposition. The grains observed in the SEM micrographs are formed by coalescence of small crystallites as estimated from p-XRD analysis. Interface between glass substrate and deposited ZnS thin film can be observed through cross sectional view Fig. 2(d). Film is composed of layers since there are five depositions on the same substrate. The total thickness of the film is approximately 5 μm. EDAX analysis was consistent with the deposition of ZnS (~1:1) on glass substrate along with peaks of glass constituents.

Surface roughness was studied by atomic force microscopy (AFM). AFM images (2D and 3D) presented in Fig. 3 show that the film is uniform and smooth. The uniformity and flatness of surface in case of thin films is very important from application point of view. In the present study, area of the film examined is 5 μm^2. Low values of roughness are observed in both types *i.e.* root mean square (RMS) roughness (0.4231 nm) and average roughness (0.3201 nm).

Further information on the microstructure of ZnS thin film was obtained from transmission electron microscopy (TEM), high resolution transmission electron microscopy (HRTEM) images and selected area electron diffaraction (SAED) Fig. 4. It was difficult to observe the actual size of nanoparticles in TEM due to agglomeration of particles as seen in left part of Fig. 5. HRTEM image shows that ZnS nanoparticles are of good crystallinity, and top right inset of Fig. 4 shows lattice spacing (0.30 Å) corresponding to (111) plane of cubic phase consistent with the results obtained from p-XRD. SAED pattern shows a set of rings (obtained as diffraction from different planes) instead of spots due to the smaller size of particles and polycrystalline nature of thin film. SAED pattern corresponds to the cubic phase of ZnS with (111), (220) and (311) planes.

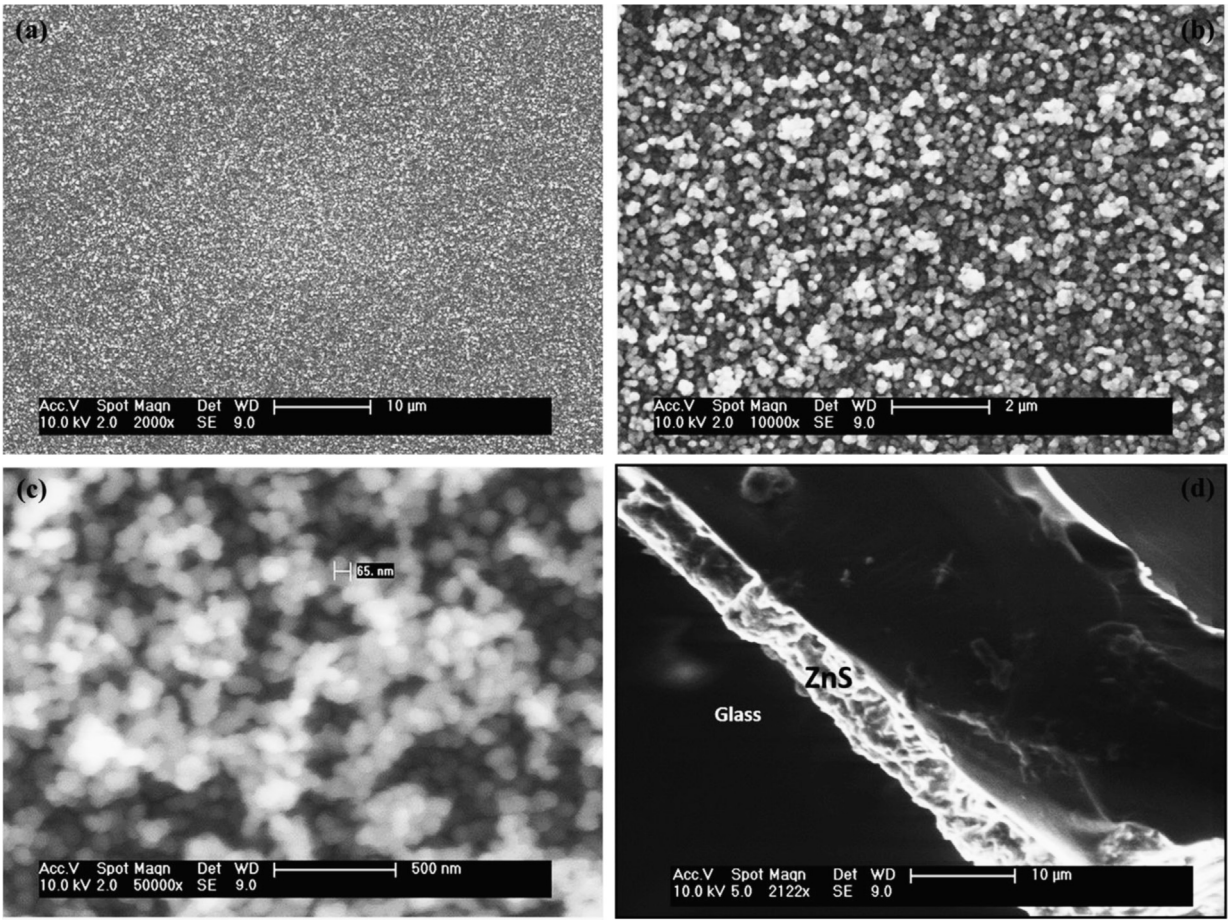

Fig. 2. (a–c) SEM micrographs at different magnifications and (d) cross sectional image of CBD-deposited ZnS film onto glass substrate using ($[Zn^{2+}]=0.15$ M, [Urea]=5 M, [Thioacetamide]=1 M, pH 4, deposition time=3 h) after fifth deposition.

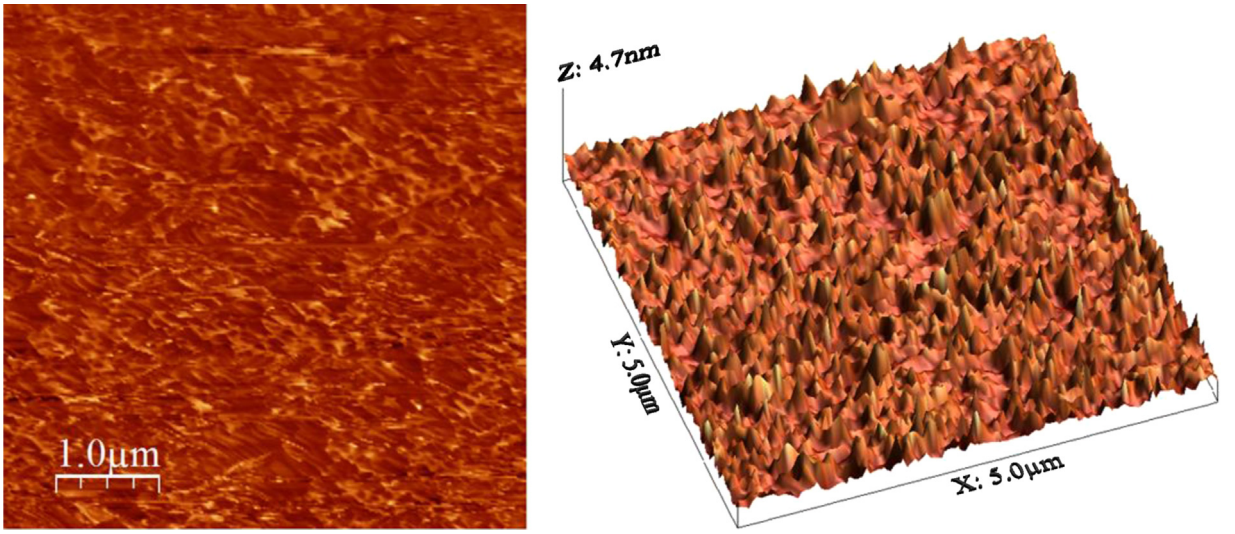

Fig. 3. AFM (2D and 3D) image of CBD-deposited ZnS film onto glass substrate using ([Zn^{2+}]=0.15 M, [Urea]=5 M, [Thioacetamide]=1 M, pH 4, deposition time=3 h) after fifth deposition.

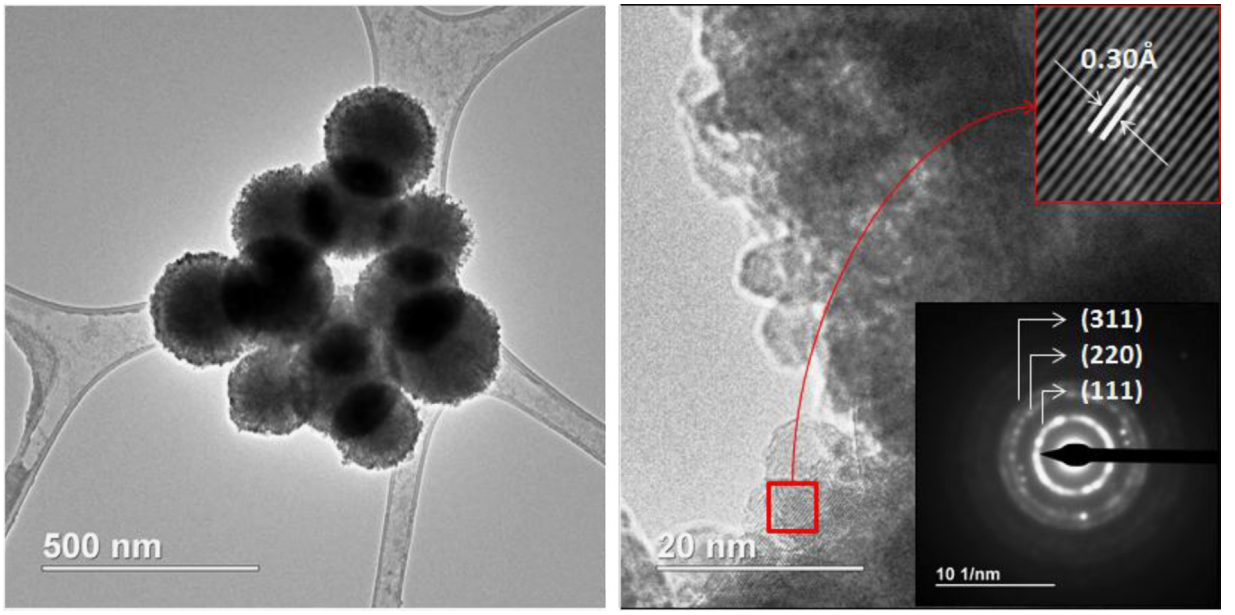

Fig. 4. TEM micrograph with SAED pattern and *d*-spacing (inset) of CBD-deposited ZnS film onto glass substrate using ([Zn^{2+}]=0.15 M, [Urea]=5 M, [Thioacetamide]=1 M, pH 4, deposition time=3 h) after fifth deposition.

X-ray photoelectron spectra obtained for films indicate the shift in binding energies of zinc (1022 eV, $2p_{3/2}$; 1044 eV, $2p_{1/2}$) and sulfur (165 eV, $2p_{1/2}$) towards higher values. This shift in binding energies can be attributed to the chemical effects along with matrix effects *i.e.* relaxation energy, work function and crystal potential [46]. Rodriguez et al. [47] explains the electronic interactions in bimetallic system in order to study shifts in binding energies of core levels. They determined the shift in binding energies depending on the number of layers on a particular substrate. Fig. 5 shows the XPS spectra of zinc and sulfur for ZnS thin film after five depositions. Inset of Fig. 6 shows the complete XPS survey of ZnS thin film. The presence of oxygen ascribed as constituent of glass substrate rather than evidence of oxide material.

3.3. Optical studies

UV–vis spectrometer was used to study the absorbance of ZnS thin films. The variation of $(\alpha h\nu)^2$ with photon energy $h\nu$ is shown in Fig. 6 and it can be seen that plot of $(\alpha h\nu)^2$ *vs.* $h\nu$ is linear over a wide range of photon energies indicating the direct type of transitions. The energy gap E_g of the ZnS thin films was evaluated by extrapolating the

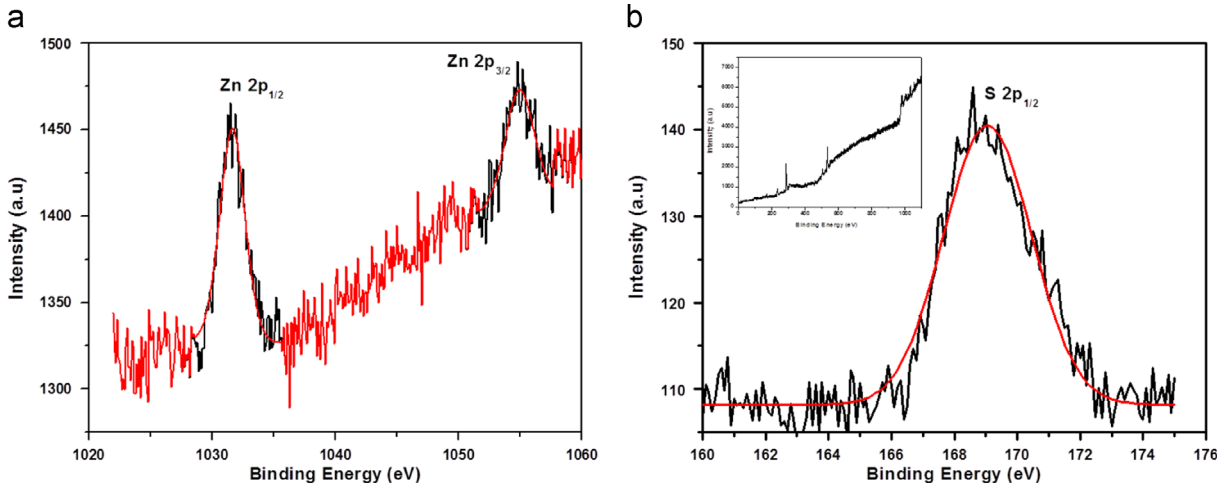

Fig. 5. XPS spectrum of CBD-deposited ZnS film onto glass substrate using ([Zn^{2+}]=0.15 M, [Urea]=5 M, [Thioacetamide]=1 M, pH 4, deposition time=3 h) after fifth deposition.

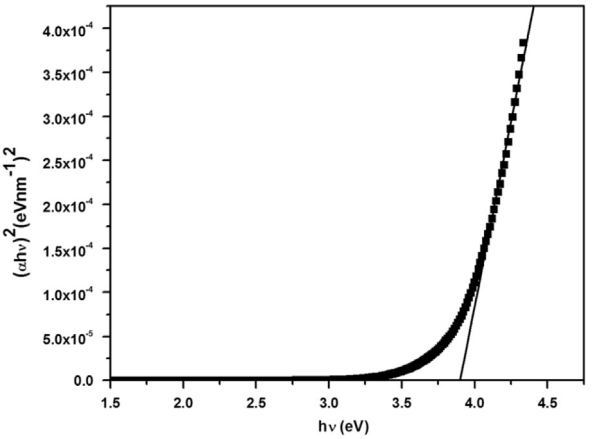

Fig. 6. Band gap plot of CBD-deposited ZnS film onto glass substrate using ([Zn^{2+}]=0.15 M, [Urea]=5 M, [Thioacetamide]=1 M, pH 4, deposition time=3 h) after fifth deposition.

linear portion of the curve and intercept on energy-axis estimates the band gap energy. The band gap (3.78 eV) being found is higher than that of bulk cubic ZnS (3.54 eV) [48] due to nanocrystalline nature of thin films. Optical results are completely in co-relation with the XRD analysis since few of the reports determined the hexagonal phase [43,45] of ZnS by the CBD method. We confirmed our results by multiple experiments and found that the results being presented can be reproduced.

The transmittance and absorbance plots (Fig. 7) show 70–90% transmittance in the visible region. Fig. 7 also shows the variation of refractive index of ZnS thin film as a function of wavelength, the inset shows the optical density. ZnS thin films with high refractive index can be used as anti-reflecting coatings in optoelectronic devices (solar cells). The photoluminescence of ZnS thin film was studied at room temperature with an excitation wavelength of 340 nm. Emission spectrum of the ZnS thin film after five

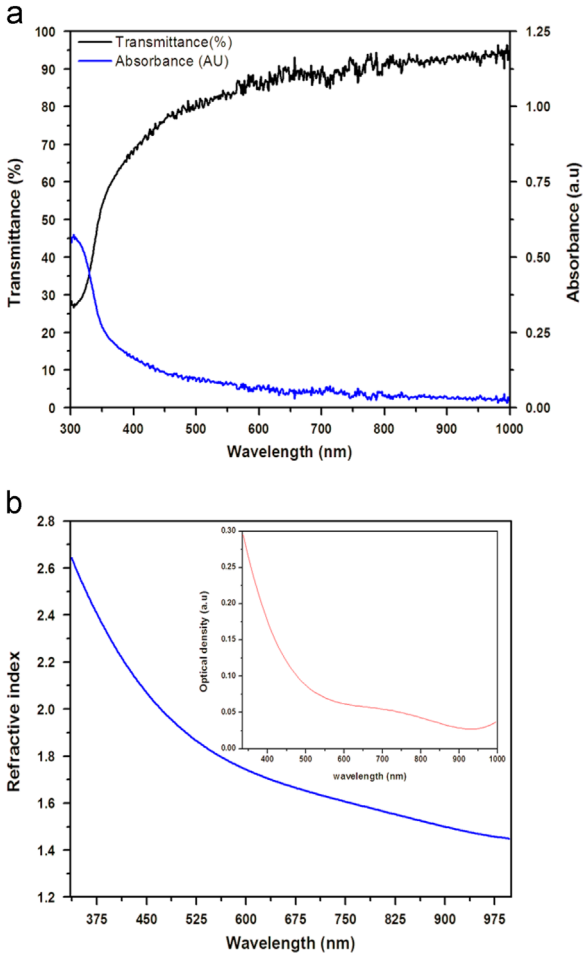

Fig. 7. (a) Transmittance and absorbance, (b) refractive index and optical density (inset) of CBD-deposited ZnS film on glass substrate using ([Zn^{2+}]=0.15 M, [Urea]=5 M, [Thioacetamide]=1 M, pH 4, deposition time=3 h) after fifth deposition.

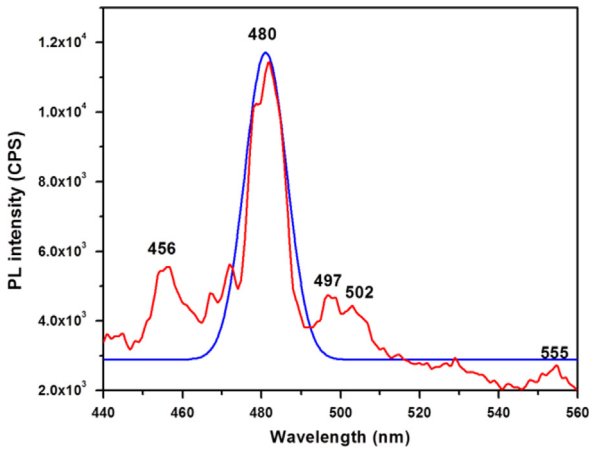

Fig. 8. PL of CBD-deposited ZnS film onto glass substrate using ($[Zn^{2+}]$= 0.15 M, [Urea]=5 M, [Thioacetamide]=1 M, pH 4, deposition time=3 h) after fifth deposition.

depositions is shown in Fig. 8. Broad peak centered at 480 nm attributed to the nanocrystalline nature of ZnS film with large size distribution. Green emission at 555 nm which represent the characteristic peak of ZnS is found to be suppressed in this case. Blue shift in the emission might be attributed to the defect states and sulfur vacancies.

4. Conclusions

The growth of nanocrystalline ZnS thin film have been optimized in a chemical bath deposition onto glass substrates. p-XRD reveals that these nanocrystalline thin films are cubic (zinc blende) in nature. SEM, EDAX, XPS and UV–vis results are consistent with the XRD data and show the nanocrystalline nature of thin films without any evidence of impurities. The films show high crystallinity, good adhesion and minimum reflection in the visible region and hence have potential applications in optoelectronic or solar cell devices.

Acknowledgment

One of the authors (M. Saeed Akhtar) would like to acknowledge the Higher Education Commission (HEC) of Pakistan for providing financial support as indigenous scholarship (Grant no. 17-5-4(Ps4-264)/HEC/Sch/2007) in Batch-IV and IRSIP scholarship (Grant no. 1-8/HEC/HRD/2013/2503). We also thank EPSRC for funding of instruments under grant number EP/K039547/1 for characterization of the compounds.

References

[1] X.Z. Ye, Y. Li, J.Y. Dong, J.Y. Xiao, Y.R. Ma, L.M. Qi, J. Mater. Chem. C 1 (38) (2013) 6112.
[2] G. Turgut, E.F. Keskenler, S. Aydin, S. Dogan, S. Duman, E. Sonmez, B. Esen, B. Duzgun, Mater. Lett. 102 (2013) 106.
[3] A. Short, L. Jewell, S. Doshay, C. Church, T. Keiber, F. Bridges, S. Carter, G. Alers, J. Vac. Sci. Technol. A 31 (1) (2013).
[4] S. Kubota, K. Kanomata, K. Momiyama, T. Suzuki, F. Hirose, IEICE Trans. Electron. E96c (4) (2013) 604.
[5] A.C. Dhanya, K.V. Murali, K.C. Preetha, K. Deepa, A.J. Ragina, T.L. Remadevi, Mater. Sci. Semiconduct. Process. 16 (3) (2013) 955.
[6] J. Mann, J. Li, I. Repins, K. Ramanathan, S. Glynn, C. DeHart, R. Noufi, IEEE J. Photovolt. 3 (1) (2013) 472.
[7] H. Ramli, S.K.A. Rahim, T. Abd Rahim, M.M. Aminuddin, Chalcogenide Lett. 10 (6) (2013) 189.
[8] G. Kedawat, S. Srivastava, V.K. Jain, P. Kumar, V. Kataria, Y. Agrawal, B.K. Gupta, Y.K. Vijay, ACS Appl. Mater. Inter. 5 (11) (2013) 4872.
[9] Y.C. Han, M.S. Lim, J.H. Park, K.C. Choi, Org. Electron. 14 (12) (2013) 3437.
[10] J. Vidal, O. de Melo, O. Vigil, N. Lopez, G. Contreras-Puente, O. Zelaya-Angel, Thin Solid Films 419 (1–2) (2002) 118.
[11] T.A. Safeera, K.J. Anju, P.J. Joffy, E.I. Anila, AIP Conf. Proc. 1512 (2013) 668.
[12] X. Zeng, S.S. Pramana, S.K. Batabyal, S.G. Mhaisalkar, X.D. Chen, K.B. Jinesh, Phys. Chem. Chem. Phys. 15 (18) (2013) 6763.
[13] X.M. Wang, C.Q. Yu, J.X. Wu, Z.H. Wei, Y.D. Zhang, Asian J. Chem. 25 (3) (2013) 1241.
[14] Y.D. Zhang, L.W. Mi, Chem. Lett. 41 (9) (2012) 915.
[15] A. Fischereder, M.L. Martinez-Ricci, A. Wolosiuk, W. Haas, F. Hofer, G. Trimmel, G.J.A.A. Soler-Illia, Chem. Mater. 24 (10) (2012) 1837.
[16] W. Zhang, X.H. Zeng, J.F. Lu, H.T. Chen, Mater. Res. Bull. 48 (10) (2013) 3843.
[17] M. Ashrat, M. Mehmood, A. Qayyum, Semiconductors 46 (10) (2012) 1326.
[18] Y.G. Yoon, I.H. Choi, J. Korean Phys. Soc. 63 (8) (2013) 1609.
[19] D. Yoo, M.S. Choi, S.C. Heo, C. Chung, D. Kim, C. Choi, Met. Mater. Int. 19 (6) (2013) 1309.
[20] D. Yoo, M.S. Choi, C. Chung, S.C. Heo, D. Kim, C. Choi, J. Nanosci. Nanotechnol. 13 (12) (2013) 7814.
[21] X.H. Xu, F. Wang, Z.L. Li, J.J. Liu, J. Ji, J.F. Chen, Electrochim. Acta 87 (2013) 511.
[22] H.M.M.N. Hennayaka, H.S. Lee, Thin Solid Films 548 (2013) 86.
[23] M. Zhou, D.Q. Liu, T.Y. Yu, Q.Y. Cai, in: Proceedings of the 6th International Symposium on Advanced Optical Manufacturing and Testing Technologies: Optoelectronic Materials and Devices for Sensing, Imaging, and Solar Energy, vol. 8419, 2012.
[24] M.A. Ehsan, T.A.N. Peiris, K.G.U. Wijayantha, H. Khaledi, H.N. Ming, M. Misran, Z. Arifin, M. Mazhar, Thin Solid Films 540 (2013) 1.
[25] K. Ramasamy, M.A. Malik, M. Helliwell, J. Raftery, P. O'Brien, Chem. Mater. 23 (6) (2011) 1471.
[26] G.L. Agawane, S.W. Shin, M.S. Kim, M.P. Suryawanshi, K.V. Gurav, A. V. Moholkar, J.Y. Lee, J.H. Yun, P.S. Patil, J.H. Kim, Curr. Appl. Phys. 13 (5) (2013) 850.
[27] Z.Y. Zhong, E.S. Cho, S.J. Kwon, Mater. Chem. Phys. 135 (2–3) (2012) 287.
[28] T. Iwashita, S. Ando, Thin Solid Films 520 (24) (2012) 7076.
[29] P.U. Bhaskar, G.S. Babu, Y.B.K. Kumar, Y. Jayasree, V.S. Raja, Mater. Chem. Phys. 134 (2–3) (2012) 1106.
[30] G.L. Agawane, S.W. Shin, A.V. Moholkar, K.V. Gurav, J.H. Yun, J.Y. Lee, J.H. Kim, J. Alloys Compd. 535 (2012) 53.
[31] J. McAleese, P. O'Brien, Thin-Film Structures for Photovoltaics, 485, 255.
[32] I.O. Oladeji, L. Chow, Thin Solid Films 339 (1–2) (1999) 148.
[33] P. O'Brien, M.R. Heinrich, D.J. Otway, O. Robbe, A. Bayer, D.S. Boyle, Chemical Processing of Dielectrics, Insulators and Electronic Ceramics, 606, 199.
[34] A. Bayer, D.S. Boyle, P. O'Brien, J. Mater. Chem. 12 (10) (2002) 2940.
[35] Q.Y. Zhang, E.S.M. Goh, R. Beuerman, Z. Judeh, M.B. Chan-Park, T. P. Chen, R. Xu, J. Appl. Polym. Sci. 129 (4) (2013) 1793.
[36] P.A. Luque, M.A. Quevedo-Lopez, A. Olivas, Mater. Lett. 106 (2013) 49.
[37] A.X. Wei, J. Liu, M.X. Zhuang, Y. Zhao, Mater. Sci. Semicond. Process. 16 (6) (2013) 1478.
[38] K. Shinoda, T. Arai, H. Ohshima, B. Jeyadevan, A. Muramatsu, K. Tohji, E. Matsubara, Mater. Trans. 43 (7) (2002) 1512.
[39] F. Long, W.M. Wang, Z.K. Cui, L.Z. Fan, Z.G. Zou, T.K. Jia, Chem. Phys. Lett. 462 (1–3) (2008) 84.
[40] P. O'Brien, J. McAleese, J. Mater. Chem. 8 (11) (1998) 2309.
[41] J. Vidal, O. Vigil, O. de Melo, N. Lopez, O. Zelaya-Angel, Mater. Chem. Phys. 61 (2) (1999) 139.
[42] L.M. Zhou, N. Tang, S.M. Wu, Surf. Coat. Technol. 228 (2013) S146.
[43] L.Y. Chen, C. Fang, Appl. Mech. Mater. 281 (2013) 523.
[44] S.M. Salim, A.H. Eid, A.M. Salem, H.M. Abou El-Khair, Surf. Interface Anal. 44 (8) (2012) 1214.
[45] S.W. Shin, G.L. Agawane, M.G. Gang, A.V. Moholkar, J.H. Moon, J. H. Kim, J.Y. Lee, J. Alloys Compd. 526 (2012) 25.
[46] K.S. Kim, N. Winograd, Chem. Phys. Lett. 30 (1) (1975) 91.
[47] J.A. Rodriguez, R.A. Campbell, D.W. Goodman, J. Vac. Sci. Technol. A 9 (3) (1991) 1698.
[48] G.L.E. Turner, Ann. Sci. 48 (5) (1991) 496.